Challenges of diagnosing glaucoma in myopic eyes

Qiu, Kunliang

Chapter 5

Determinants of the retinal nerve fiber layer profile in myopic eyes: a separate analysis of the superior and inferior hemiretina

Kunliang Qiu, Xuehui Lu, Geng Wang, Riping Zhang, Mingzhi Zhang, Nomdo M. Jansonius

In revision of Scientific Reports

ABSTRACT

The peripapillary retinal nerve fiber layer (RNFL) thickness profile differs between myopic and nonmyopic eyes and may differ between the superior and inferior hemiretina. This hampers the use of OCT derived RNFL thickness measurements in glaucoma. We imaged the peripapillary RNFL of 138 eyes from 138 healthy myopic subjects with the Cirrus HD OCT and determined the location (angle) of the superior and inferior peak of the RNFL thickness profile at the 3.46 mm OCT measurement circle. We determined associations between the superior and inferior RNFL peak thickness angle and the ocular factors axial length, the angles of the supratemporal and infratemporal retinal artery and vein, disc area, fovea-disc angle [FDA], disc ovality index, and disc torsion using multiple linear regression. In the superior hemiretina, the RNFL peak thickness angle was associated with the superior artery angle ($P<0.001$), superior vein angle ($P<0.001$), disc area ($P=0.003$), FDA ($P=0.012$), and disc torsion ($P=0.004$). In the inferior hemiretina, the RNFL peak thickness angle was associated with axial length ($P=0.025$), inferior artery angle ($P<0.001$), inferior vein angle ($P=0.010$), and FDA ($P<0.001$). Our findings indicate that the myopic RNFL thickness profile is determined by different ocular parameters in the superior and inferior hemiretina.

Introduction

Glaucoma is a progressive optic neuropathy characterized by damage of retinal ganglion cells and their axons. With recent advances of the optical coherence tomography (OCT) technology, in vivo measurement of retinal nerve fiber layer (RNFL) thickness has been shown emerging as an important diagnostic technology for glaucoma (Sommer et al., 1991; Huang et al., 1991; Medeiros et al., 2005; Banister et al., 2016). However, considerable anatomic variation of the RNFL thickness profile has been reported, which may confound the assessment of glaucoma (Ghadiali et al., 2008; Shin et al., 2015; Brito et al., 2015; Hwang et al., 2012; Yamashita et al., 2013; Choi et al., 2014).

Myopia is a prevalent ocular morbidity and a major risk factor for glaucoma (Williams et al., 2015; Marcus et al., 2011). Thus, understanding of characteristics and determinants of the retinal nerve fiber layer profile in myopia is of great importance for glaucoma assessment. Previous studies have shown that the peripapillary RNFL profile was influenced by myopia status, tilted disc, and retinal blood vessel topography (Shin et al., 2015; Brito et al., 2015; Hwang et al., 2012; Yamashita et al., 2013; Choi et al., 2014). However, our understanding of the RNFL thickness profile variability in myopic eyes is incomplete. As myopic eyes are likely to have tilted discs and narrower retinal artery trajectories (Tay et al., 2005; Yamashita et al., 2014), it is uncertain whether myopia alone affects the RNFL profile, or in combination with optic disc anatomy and/or retinal blood vessel topography. Furthermore, different globe shape, including spheroidal, ellipsoidal, conical, nasally distorted, temporally distorted, and barrel shapes have been reported in myopia especially high myopia (Guo et al., 2017). During myopia development, the asymmetrical elongation of the globe could cause a difference in the RNFL thickness profile between the superior and inferior hemiretina. Therefore, it would be important and helpful to address the influences of various parameters on the variability of the profile in the superior and inferior hemiretina separately.

The aim of this study was to determine the characteristics and determinants of the peripapillary RNFL thickness profile of healthy myopic eyes. For this purpose, we performed a cross-sectional study in a large group of myopic subjects and evaluated the effects of various ocular factors (including axial length, disc area, fovea-disc angle [FDA], disc ovality, disc torsion, and retinal blood vessel topography) on the variability of RNFL thickness profile in the superior and inferior hemiretina.

Methods

Subjects

One hundred and forty seven Chinese myopic subjects were consecutively recruited from the refractive surgery clinic of Joint Shantou International Eye Center. They received a complete ophthalmic examination including a cycloplegic refraction using an autorefractor (Canon FK-1; Canon, Tokyo, Japan), a measurement of visual acuity, intraocular pressure (IOP), and axial length (IOL Master; Carl-Zeiss Meditec, Dublin, CA), a visual field test (see below), and a dilated stereoscopic fundus examination. Apart from the refractive error, the included eyes were free of ocular disease. Subjects were excluded if the IOP was above 21 mmHg, the best corrected visual acuity was less than 20/40, if they had a family history of glaucoma, or if they had a history of myopic macular degeneration, refractive surgery, intraocular surgery, diabetes, neurological disease, or glaucoma. One eye from each subject was randomly selected. All the included eyes had a spherical equivalent less than -0.5 diopters (D). The present study followed the tenets of the declaration of Helsinki and was approved by the local ethical committee. Written informed consent was obtained from each subject before enrolment.

Visual field testing

All the included eyes received visual field tests with standard automated perimetry using the 24-2 grid and the SITA standard strategy (Humphrey Field Analyzer II; Carl Zeiss Meditec, Inc.). Only reliable visual field tests (with fixation loss less than 20% and false positive and negative less than 10%) were included in the analysis (Bengtsson & Heijl 2000; Junoy et al., 2012). All the included visual field tests had a pattern standard deviation (PSD) *p* value > 5% and were within normal limits according to the glaucoma hemifield test (GHT).

Optical coherence tomography

Each of the included eyes received RNFL imaging using the Cirrus High Definition OCT (software version 5.0.0.326; Carl Zeiss Meditec, Dublin, CA). The axial resolution of this OCT device is 5 μm and the scan speed 27,000 A-scans per second (Carl Zeiss 2008). Both the Macular Cube 512×128 protocol and the Optic Disc Cube 200×200 protocol were performed. Measurements with eye movements during image acquisition (checked by reviewing the real-time SLO fundus images) were excluded and retaken. Each included image had minimum signal strength of 7 (median 8).

Measurement of RNFL peak thickness angles

RNFL thickness maps were generated with the built-in software of the Cirrus HD-OCT and subsequently exported to a personal computer for further analysis. The locations of the peaks in the RNFL thickness profile were determined on the temporal, superior, nasal, inferior, and temporal (TSNIT) thickness curve as measured on the 3.46 mm diameter measurement circle, which is centered around the center of the optic disc. The superior and inferior RNFL peak thickness angle were measured in degrees relative to the horizontal meridian (Figure 1A). We also calculated the total peak thickness angle (angle between the superior and inferior peak).

Measurement of disc area and adjustment for ocular magnification

The disc area was derived from the analysis printout by the automatic built-in software. According to previous studies, the actual area measurements on fundus pictures in myopic eyes need to take into consideration of ocular magnification. Based on the Bennett's method (Bennet et al., 1994), the relationship between the measured and actual OCT area can be expressed as:

$$t^2 = p^2 \times q^2 \times s^2, \quad (1)$$

where t is the actual fundus dimension, p is the magnification factor of the camera of the HD-OCT system, q the magnification factor of the eye, and s the measurement obtained from the OCT system. For the OCT device used in this study, p is known to be 3.382 (Kang et al., 2010). The magnification factor of the eye can be calculated with the formula:

$$q = 0.01306 \times (AL - 1.82), \quad (2)$$

where AL is the axial length in mm. Thus, the corrected disc area can be calculated by the following formula:

$$A_c = 3.382^2 \times 0.01306^2 \times (AL\text{-}1.82)^2 \times A_m, \quad (3)$$

where A_c is the corrected area and A_m the measured area. The corrected disc area was used in the analysis.

Measurement of the fovea-disc angle (FDA)

Measurement of the FDA was performed with ImageJ software (available in the public domain at http://rsbweb.nih.gov/ij/; www.nih.gov, National Institutes of Health, Bethesda, MD, USA), based on the coordinates of the fovea and the center of the optic disc.[31] The fovea and optic disc center were automatically detected by the OCT software on the SLO fundus image with overlayed macular color thickness map and RNFL thickness deviation map, respectively. Both were

exported and manually registered to each other (Figure 1B) with Illustrator CS4 software (Adobe Systems Inc., San Jose, California). To make a good registration, the retinal vessel trajectories were used as a reference and the transparency of the optic disc image was set to 50% to allow visualization of the underlying SLO fundus image.

The FDA was defined as the angle between the disc-fovea line and the horizontal (Figure 1B). A positive FDA value indicates that the fovea is located inferiorly with respect to the optic disc center.

Measurement of major retinal blood vessel angles

Measurements of the major temporal retinal blood vessels angles were performed using the OCT RNFL deviation map (Fig. 1C). The intersections of the superotemporal and inferotemporal artery and vein with the 3.46 mm OCT measurement circle were manually determined by one investigator (KQ). Subsequently, the artery and vein angles were defined as the angle between the horizontal meridian and a line through the disc center and the intersections of the vessels with the measurement circle.

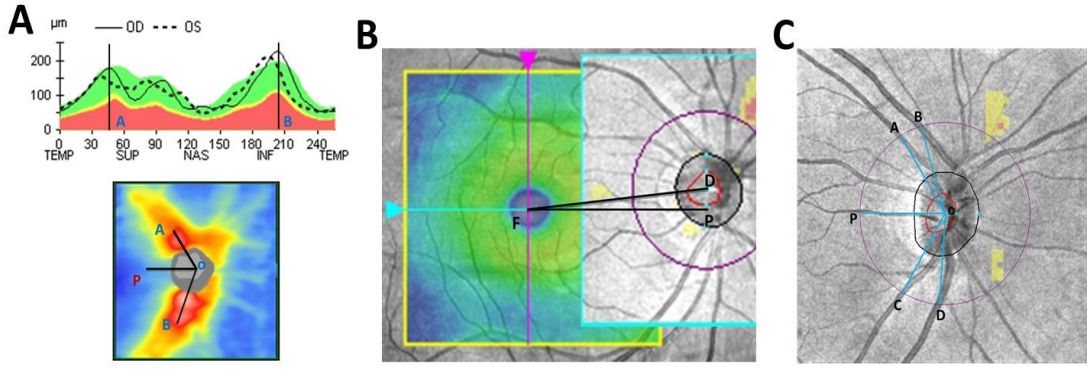

Figure 1. Definitions of superior/inferior RNFL peak thickness angle (A), fovea-disc angle (B), and retinal vascular topography (C). For details see Methods section.

Confocal scanning laser ophthalmoscopy imaging - disc ovality index and disc torsion

The optic disc of each eye was also imaged with confocal scanning laser ophthalmoscopy (Heidelberg Retina Tomograph II [HRT 2]; Heidelberg Engineering, GmbH, Dossenheim, Germany). A three-dimensional topographic image consisting of 384×384×16 up to 384×384×64 pixels is constructed from multiple focal planes axially along the optic nerve head. Three consecutive scans were obtained and aligned to compose a single mean topography for analysis. All the optic disc images were checked carefully for image quality. Only images with an average pixel height standard deviation of no more than 30 μm were included in the analysis. The contour lines were manually drawn by a trained ophthalmologist (KQ). The margin of the optic disc was defined as the inner edge of the Elschnig's ring.

By using the ImageJ software, the optic disc images from the HRT 2 topographic analysis report were exported for further analysis. The definitions of optic disc ovality and optic disc torsion have been described elsewhere (Takasaki et al., 2013; Park et al. 2012). Briefly, optic disc ovality was quantified using the disc ovality index (defined as the shorter diameter divided by the longer diameter). Disc torsion was defined as the deviation (in degree) of the long axis of the optic disc from the vertical reference (a line perpendicular to the line connecting the disc center and the fovea). An inferotemporally directed torsion (counterclockwise torsion in the right eye format) was presented as a positive value, while a superonasally directed torsion (clockwise torsion in the right eye format) was presented as a negative value.

Statistical Analysis

Univariable and multivariable analysis (Pearson's correlation analysis and multiple linear regression) were performed to determine the associations between the determinants and the superior, inferior, and total RNFL peak thickness angle.

All statistical analyses were performed with the SPSS software (ver. 17.0; SPSS Inc, Chicago, IL). A P value of 0.05 or less was considered statistically significant.

Results

Of the 147 screened subjects, nine subjects were excluded because of unreliable visual field tests (6 subjects) or poor OCT scan quality (3 subjects). As a result, 138 eyes from 138 subjects (60 females and 89 right eyes) were finally included in the analysis. Table 1 presents the demographics of the study population. The mean (SD; range) axial length and refractive error were 25.6 (1.1; 22.5 to 28.8) mm and -5.1 (2.3; -9.6 to -0.5) D, respectively.

Table 1. Characteristics of the Study Population (n=138)

	Median (interquartile range)	Range
Age, y	22.5 (20.7 to 24.1)	18 to 40
Spherical equivalent, D	-4.88 (-6.69 to -3.72)	-15.75 to -0.50
Axial length, mm	25.60 (24.86 to 26.30)	22.52 to 28.77
Mean deviation of visual field, dB	-2.21 (-2.80 to -1.56)	-4.96 to 1.47
Disc area, mm^2	1.88 (1.68 to 2.17)	1.12 to 3.40
FDA, deg	5.0 (3.4 to 8.0)	-1.1 to 15.8
Disc ovality index	0.82 (0.76 to 0.89)	0.60 to 1.00
Disc torsion degree, deg	3.2 (-7.7 to 15.1)	-77.4 to 87.1
Superior vein angle, deg	66.8 (56.9 to 75.6)	37.0 to 92.6
Superior artery angle, deg	65.6 (58.7 to 71.8)	38.3 to 88.5
Inferior vein angle, deg	68.2 (58.6 to 83.2)	35.4 to 104.0
Inferior artery angle, deg	66.2 (59.2 to 74.5)	32.6 to 113.9
Total vein angle, deg	136.8 (121.0 to 150.6)	73.3 to 189.1
Total artery angle, deg	132.1 (121.0 to 144.0)	84.4 to 193.4
Average RNFL thickness, μm	98.0 (90.8 to 103.0)	81.0 to 128.0
Superior RNFL peak thickness angle, deg	62.6 (56.3 to 68.9)	38.0 to 122.3
Inferior RNFL peak thickness angle, deg	62.6 (56.8 to 68.4)	40.8 to 99.8
Total RNFL peak thickness angle, deg	125.2 (115.3 to 136.4)	84.4 to 194.1

Table 2 demonstrates the associations between the determinants and the superior, inferior, and total RNFL peak thickness angle. The superior RNFL peak thickness angle correlated significantly with disc area, FDA, disc ovality index, disc torsion, superior artery angle, and superior vein angle. The inferior RNFL peak thickness angle correlated significantly with axial length, refractive error, FDA, inferior artery angle, and inferior vein angle. The total RNFL peak thickness angle correlated significantly with axial length/refractive error, disc area, disc ovality, disc torsion, total artery angle, and total vein angle. Figure 2 shows the relationships between the superior and inferior RNFL peak thickness angle and axial length and FDA.

Table 2. Factors associated with superior, inferior, and total RNFL peak thickness angle – univariable analysis

	Superior peak angle		Inferior peak angle		Total peak angle	
	r	P	r	P	r	P
Axial length	-0.15	0.079	-0.35	<0.001	-0.30	<0.001
Spherical equivalent	0.16	0.060	0.25	0.003	0.26	0.002
Disc area	0.34	<0.001	0.13	0.129	0.30	<0.001
FDA	-0.34	<0.001	0.39	<0.001	-0.02	0.78
Disc ovality index	0.31	<0.001	-0.07	0.424	0.26	0.002
Disc torsion	0.25	0.004	-0.08	0.347	0.20	0.017
Superior artery angle	0.68	<0.001	/	/	/	/
Superior vein angle	0.47	<0.001	/	/	/	/
Inferior artery angle	/	/	0.56	<0.001	/	/
Inferior vein angle	/	/	0.40	<0.001	/	/
Total artery angle	/	/	/	/	0.75	<0.001
Total vein angle	/	/	/	/	0.55	<0.001

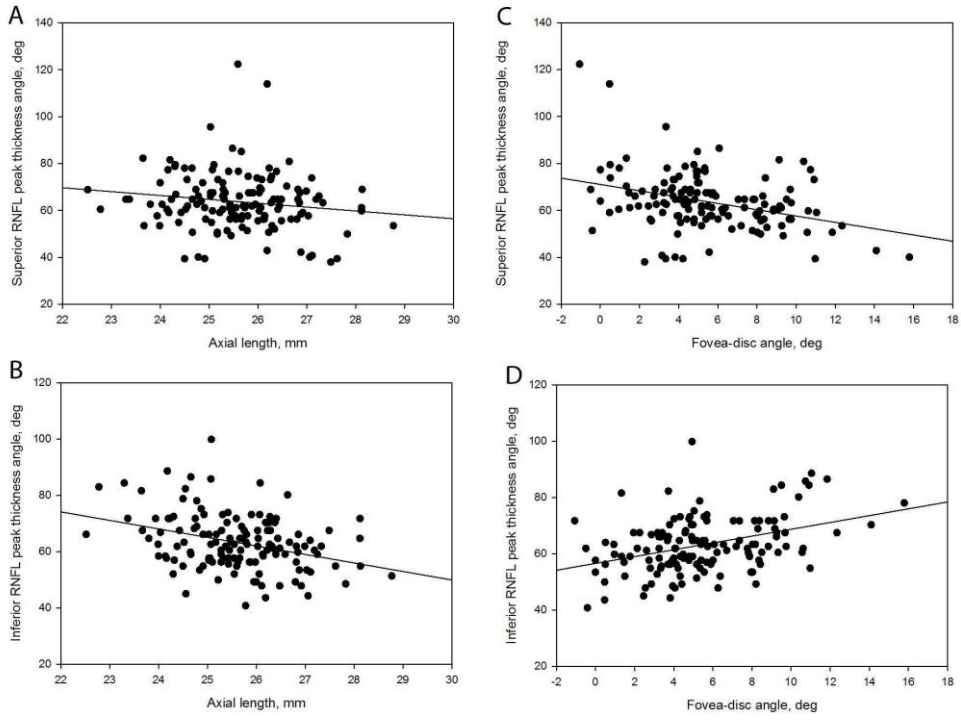

Figure 2. Scatterplots showing the relationship between axial length (left column) and fovea-disc angle (right column) and the RNFL peak thickness angle in the superior and inferior hemiretina. A: superior RNFL peak thickness angle versus axial length (r=-0.15, P=0.079); B: inferior RNFL peak thickness angle versus axial length (r=-0.35, P<0.001); C: superior RNFL peak thickness angle versus fovea-disc angle (r=-0.34, P<0.001); D: inferior RNFL peak thickness angle versus fovea-disc angle (r=0.39, P<0.001).

In the multivariable analysis, a smaller superior RNFL peak thickness angle was significantly associated with a smaller superior artery angle, smaller superior vein angle, smaller optic disc area, a larger FDA, and a greater disc torsion (Table 3A). A smaller inferior RNFL peak thickness angle was significantly associated with a smaller inferior artery angle, smaller inferior vein angle, longer axial length, and smaller FDA (Table 3B). A smaller total RNFL peak thickness angle was significantly associated with a smaller total artery angle and a smaller total vein angle (Table 3C). Of all determinants, the artery angle was the most prominent predictor of the observed variability, for both hemiretinae (R^2 of models with only the arterial angle included were 0.46 and 0.31 for the superior and inferior hemiretina, respectively).

Table 3. Factors associated with superior, inferior, and total RNFL peak thickness angle (deg) – multivariable analysis

	R^2	β coefficient	P
A. Superior RNFL peak angle	0.63		
Superior artery angle (deg)		0.68	<0.001
Superior vein angle (deg)		0.27	<0.001
Disc area (mm^2)		5.25	0.003
FDA (deg)		-0.57	0.012
Disc torsion (deg)		-0.08	0.004
B. Inferior RNFL peak angle	0.47		
Inferior artery angle (deg)		0.36	<0.001
Inferior vein angle (deg)		0.12	0.010
Axial length (mm)		-1.35	0.025
FDA (deg)		0.77	<0.001
C. Total RNFL peak angle	0.67		
Total artery angle (deg)		0.60	<0.001
Total vein angle (deg)		0.27	<0.001

Discussion

In myopia, the peripapillary RNFL thickness profile is determined by different ocular parameters in the superior and inferior hemiretina. In the superior hemiretina, the superior artery angle, superior vein angle, optic disc area, FDA, and disc torsion contribute to this variability; in the inferior hemiretina, the contributing factors are the inferior artery angle, inferior vein angle, axial length, and FDA. Of all determinants, the artery angle appears to be the most prominent predictor of the observed variability, for both hemiretinae.

The peripapillary RNFL thickness profile in myopic eyes has been addressed previously (Kim et al., 2010; Wang et al., 2011; Leung et al., 2012; Yamashita et al., 2017; Hong et al., 2010). The temporal RNFL has been reported to be thicker in myopic eyes than in nonmyopic eyes (Kim et al., 2010; Wang et al., 2011). By analysing the radial axes of the superotemporal and inferotemporal RNFL bundles as determined in the RNFL thickness map, Leung et al. (2012) reported that the superotemporal and inferotemporal RNFL bundles tend to shift towards the horizontal meridian with increasing myopia. In a recent study, Yamashita et al. (2017) found that the axial length was significantly associated with the RNFL peak thickness angle in the inferior hemiretina but not in the superior hemiretina. This is in agreement with our findings (Figure 2A,B; Table 3). The reason why axial length affects the RNFL thickness profile more pronounce in the inferior hemiretina remains to be uncovered. One possible explanation could be the different globe shapes in myopic eyes. It has been reported that high myopic globes demonstrate a symmetrical or asymmetrical anteroposterior elongation and posterior protrusion (Moriyama et al., 2011), which may result in various globe shapes including ellipsoidal, spheroidal, conical, nasally distorted, temporally distorted, and barrel shapes (Guo et al., 2017). It is speculated that there could be a asymmetrical dragging (asymmetrical stretching of the posterior fundus) of the retinal nerve fiber bundles towards the temporal region between the superior and the inferior hemiretina, during the elongation of the globe.

The relationship between retinal vessel topography and variability of the RNFL has been studied previously as well (Yamashita et al., 2013; Resh et al., 2011; Pereira et al., 2014; Pereira et al., 2015a; Pereira et al., 2015b; Qiu et al., 2015; Yamashita et al., 2017). Yamashita et al. demonstrated that the retinal artery angle was significantly associated with the RNFL peak thickness angle in 50 healthy subjects (Yamashita et al., 2013). We found previously that the retinal blood vessel topography was a significant determinant of the retinal nerve fiber bundle trajectory variability in the human retina (Qiu et al., 2015). Consistent with this previous study, we found that the artery and vein angles were significantly

associated with the RNFL peak thickness angle in both the superior and the inferior hemifield. Even more, we found that they were the most prominent predictors of the variability in the RNFL peak thickness angles. A possible explanation for the strong relationship between retinal vessel topography and RNFL anatomy is the fact that the vessels and nerves tend to develop in relative proximity during embryological development, possibly because they share common guidance signals (Eichmann et al., 2005; Dorrell et al., 2006).

The association between the FDA and the RNFL distribution is an area of much recent interest (Choi et al., 2014; Pereira et al., 2015b; Mwanza et al., 2016; Resch et al., 2016; Amini et al., 2014). Choi et al. (2014) demonstrated that the FDA was significantly associated with a vertical asymmetry of the RNFL distribution, in 164 healthy myopic subjects. In another recent study, however, Resch et al. (2016) reported that rotation of the RNFL measurements according to the FDA did not reduce the intersubject variability of the RNFL thickness. In the present study, we found that a larger FDA was significantly associated with a smaller superior RNFL peak thickness angle and a larger inferior RNFL peak thickness angle (Fig. 2C and D). In line with these associations, the FDA was not significantly associated with the total RNFL peak thickness angle (Table 2). Our findings agree well with previous studies (Mwanza et al., 2016; Amini et al., 2014). In Amini's and Mwanza's studies, average and regional RNFL thickness were recalculated after adjusting the FDA. With adjustment of FDA, they found a significant change of the regional but - obviously - not average RNFL thickness. On the basic of these findings, we speculate that significant rotation of RNFL profile exist in eyes with a large FDA (more inferiorly located fovea). It is important to note that current findings may not apply to OCT devices (such as the Spectralis OCT [Heidelberg Engineering, Inc., Heidelberg, Germany]) with FDA alignment (Valverde-Megías et al., 2013). No significant association between the FDA and the superior/inferior RNFL peak thickness angle remained if we repeated the analysis by using FDA adjusted RNFL peak thickness angles (superior hemifield: r=-0.09, P=0.28 after adjustment and -0.34, P<0.001before

adjustment; inferior hemifield: r=0.07, P=0.38, after adjustment and 0.39, P<0.001 before adjustment [Table 2]).

The influence of optic disc anatomy on the RNFL thickness profile has been studied widely (Shin et al., 2015; Hwang et al., 2012; Lee et al., 2014; Sung et al., 2016; Law et al., 2010). Eyes with an inferotemporal disc torsion tend to have a temporalized superior RNFL peak thickness angle (Lee et al., 2014; Law et al., 2010). Eyes with an enlarged disc ovality or tilted disc have been reported to have a thicker temporal RNFL and a smaller RNFL peak thickness angle (Shin et al., 2015; Hwang et al., 2012). In the present study, several disc parameters including disc area, disc ovality, and disc torsion, were found to correlate with the RNFL peak thickness angles in the univariable analysis. However, as disc ovality and disc torsion are associated with axial length (Tay et al., 2005), it is important to analyze these factors with multivariable analysis. In agree with previous studies (Law et al., 2010; Lee et al., 2014), we found that eyes with an inferotemporal torsion had a smaller superior RNFL peak thickness angle. Interestingly, we found that eyes with a smaller disc area tended to have a smaller superior RNFL peak thickness angle. Although the underlying mechanism of this association is not clear, our finding fits well with previous studies (Kim et al., 2011; Qiu et al., 2011). It has been shown that eyes with a small optic disc are prone to false positive diagnostic classification of RNFL measurements, which may be related to the temporal deviated RNFL profile (Kim et al., 2011; Qiu et al., 2011).

Several limitations exist in the present study. As the RNFL bundle trajectories are curvilinear in both the superior and inferior hemifields, the RNFL peak thickness angles only provide a surrogate parameter of the entire RNFL anatomy, representing the pattern of the RNFL distribution in the peripapillary area. However, as most of the current OCT devices provide RNFL measurements in the peripapillary area, our results could be applied directly in clinical practice. Another limitation is that ocular magnification may lead to errors in the measurement of the RNFL peak thickness angles and vessel angles, because the circle size depends on magnification and neither the RNFL trajectories nor the

vessels have a purely radial course. In the present study, it was not possible to measure the magnification-adjusted RNFL peak thickness angles, as the RNFL thickness profile is provided by the built-in OCT software only at one - unadjusted - distance from the center of the optic disc. By using Bennett's formula,38 however, it is possible to evaluate the retinal vessel angles at the magnification-adjusted OCT scan circle. We re-measured the adjusted retina vessel angles and found significant but minor difference between the adjusted and unadjusted measurements (131.1^{o} vs 130.0^{o}, $p<0.001$), indicating that the influence of the non-radial course of vessels (and related to that, the RNFL trajectories), is limited.

In summary, healthy myopic eyes display a significant variability in both the superior and inferior peripapillary RNFL profile. The peripapillary RNFL thickness profile is determined by different ocular parameters in the superior and inferior hemiretina. The influence of axial length, retinal vessel topography, disc area, FDA, and disc torsion should be considered when interpreting the peripapillary RNFL profile in myopic eyes.

Reference

Amini N, Nowroozizadeh S, Cirineo N, et al. Influence of the disc-fovea angle on limits of RNFL variability and glaucoma discrimination. Invest Ophthalmol Vis Sci. 2014 Oct 9;55(11):7332-7342.

Banister K, Boachie C, Bourne R, Cook J, Burr JM, Ramsay C, Garway-Heath D, Gray J, McMeekin P, Hernández R, Azuara-Blanco A. Can Automated Imaging for Optic Disc and Retinal Nerve Fiber Layer Analysis Aid Glaucoma Detection? Ophthalmology. 2016 May;123(5):930-938.

Bengtsson B, Heijl A. False-negative responses in glaucoma perimetry: indicators of patient performance or test reliability? Invest Ophthalmol Vis Sci. 2000 Jul;41(8):2201-2204.

Bennett AG Rudnicka AR Edgar DF . Improvements on Littmann's method of determining the size of retinal features by fundus photography. Graefes Arch Clin Exp Ophthalmol. 1994;232:361-367.

Brito PN, Vieira MP, Falcão MS, Faria OS, Falcão-Reis F. Optical coherence tomography study of peripapillary retinal nerve fiber layer and choroidal thickness in eyes with tilted optic disc. J Glaucoma. 2015 Jan;24(1):45-50.

Carl Zeiss Meditec, Inc. Cirrus HD-OCT User Manual. Dublin, CA: Carl Zeiss Meditec, Inc.; 2008;4.18-9. Rev. A.

Choi JA, Kim JS, Park HY, et al. The foveal position relative to the optic disc and the retinal nerve fiber layer thickness profile in myopia. Invest Ophthalmol Vis Sci. 2014 ; 55: 1419-1426.

Dorrell MI, Friedlander M. Mechanisms of endothelial cell guidance and vascular patterning in the developing mouse retina. Prog Retin Eye Res. 2006; 25: 277-295.

Eichmann A, Makinen T, Alitalo K. Neural guidance molecules regulate vascular remodeling and vessel navigation. Genes Dev. 2005; 19: 1013-1021.

Ghadiali Q, Hood DC, Lee C, et al. An analysis of normal variations in retinal nerve fiber layer thickness profiles measured with optical coherence tomography. *J Glaucoma*. 2008 ; 17: 333-340.

Guo X, Xiao O, Chen Y, et al. Three-Dimensional Eye Shape, Myopic Maculopathy, and Visual Acuity: The Zhongshan Ophthalmic Center-Brien Holden Vision Institute High Myopia Cohort Study. Ophthalmology. 2017; 124:679-687.

Hong SW, Ahn MD, Kang SH, Im SK. Analysis of peripapillary retinal nerve fiber distribution in normal young adults. Invest Ophthalmol Vis Sci. 2010; 51:3515-3523.

Huang D, Swanson EA, Lin CP, et al. Optical coherence tomography. Science. 1991;254(5035):1178-1181.

Hwang YH, Yoo C, Kim YY. Characteristics of peripapillary retinal nerve fiber layer thickness in eyes with myopic optic disc tilt and rotation. J Glaucoma. 2012 Aug;21(6):394-400.

Junoy Montolio FG, Wesselink C, Gordijn M, Jansonius NM. Factors that influence standard automated perimetry test results in glaucoma: test reliability, technician experience, time of day, and season. Invest Ophthalmol Vis Sci. 2012 Oct 9; 53(11):7010-7017.

Kang SH, Hong SW, Im SK, Lee SH, Ahn MD. Effect of myopia on the thickness of the retinal nerve fiber layer measured by Cirrus HD optical coherence tomography. Invest Ophthalmol Vis Sci. 2010 Aug;51(8):4075-4083.

Kim MJ Lee EJ Kim TW. Peripapillary retinal nerve fibre layer thickness profile in subjects with myopia measured using the Stratus optical coherence tomography. Br J Ophthalmol . 2010;94:115-120.

Kim NR, Lim H, Kim JH, Rho SS, Seong GJ, Kim CY. Factors associated with false positives in retinal nerve fiber layer color codes from spectral-domain optical coherence tomography. Ophthalmology. 2011 Sep;118(9):1774-1781.

Law SK, Tamboli DA, Giaconi J, Caprioli J. Characterization of retinal nerve fiber layer in nonglaucomatous eyes with tilted discs. Arch Ophthalmol. 2010 ;128:141-142.

Lee KH, Kim CY, Kim NR. Variations of retinal nerve fiber layer thickness and ganglion cell-inner plexiform layer thickness according to the torsion direction of optic disc. Invest Ophthalmol Vis Sci. 2014 Feb 20;55(2):1048-1055.

Leung CK, Yu M, Weinreb RN, Mak HK, Lai G, Ye C, Lam DS. Retinal nerve fiber layer imaging with spectral-domain optical coherence tomography: interpreting the RNFL maps in healthy myopic eyes. Invest Ophthalmol Vis Sci. 2012 Oct 17;53(11):7194-7200.

Marcus MW, de Vries MM, Junoy Montolio FG, Jansonius NM. Myopia as a risk factor for open-angle glaucoma: a systematic review and meta-analysis. Ophthalmology. 2011 Oct;118(10):1989-1994

Medeiros FA, Zangwill LM, Bowd C, Vessani RM, Susanna R Jr, Weinreb RN. Evaluation of retinal nerve fiber layer, optic nerve head, and macular thickness measurements for glaucoma detection using optical coherence tomography. Am J Ophthalmol 2005; 139(1):44-55.

Moriyama M, Ohno-Matsui K, Hayashi K, et al. Topographic analyses of shape of eyes with pathologic myopia by high-resolution three-dimensional magnetic resonance imaging. Ophthalmology. 2011; 118: 1626-1637.

Mwanza JC, Lee G, Budenz DL. Effect of Adjusting Retinal Nerve Fiber Layer Profile to Fovea-Disc Angle Axis on the Thickness and Glaucoma Diagnostic Performance. Am J Ophthalmol. 2016 Jan;161:12-21.e1-2.

Park HY, Lee K, Park CK. Optic disc torsion direction predicts the location of glaucomatous damage in normal-tension glaucoma patients with myopia. Ophthalmology. 2012 Sep;119(9):1844-1851.

Pereira I, Resch H, Schwarzhans F, Wu J, Holzer S, Kiss B, Frommlet F, Fischer G, Vass C. Multivariate Model of the Intersubject Variability of the Retinal Nerve Fiber Layer Thickness in Healthy Subjects. Invest Ophthalmol Vis Sci. 2015a Aug;56(9):5290-5298.

Pereira I, Weber S, Holzer S, et al. Compensation for retinal vessel density reduces the variation of circumpapillary RNFL in healthy subjects. PLoS One. 2015b; 10: e0120378.

Pereira I, Weber S, Holzer S, et al. Correlation between retinal vessel density profile and circumpapillary RNFL thickness measured with Fourier-domain optical coherence tomography. Br J Ophthalmol. 2014 ; 98: 538-543.

Qiu K, Schiefer J, Nevalainen J, Schiefer U, Jansonius NM. Influence of the Retinal Blood Vessel Topography on the Variability of the Retinal Nerve Fiber Bundle Trajectories in the Human Retina. Invest Ophthalmol Vis Sci. 2015 Oct;56(11):6320-6325.

Qiu KL, Zhang MZ, Leung CK, et al. Diagnostic classification of retinal nerve fiber layer measurement in myopic eyes: a comparison between time-domain and spectral-domain optical coherence tomography. Am J Ophthalmol. 2011 Oct;152(4):646-653.e2.

Resch H, Brela B, Resch-Wolfslehner C, et al. Position of retinal blood vessels correlates with retinal nerve fibre layer thickness profiles as measured with GDx VCC and ECC. Br J Ophthalmol. 2011 ; 95: 680-684.

Resch H, Pereira I, Hienert J, Weber S, Holzer S, Kiss B, Fischer G, Vass C. Influence of disc-fovea angle and retinal blood vessels on interindividual variability of circumpapillary retinal nerve fibre layer. Br J Ophthalmol. 2016 Apr;100(4):531-6.

Shin HY, Park HY, Park CK. The effect of myopic optic disc tilt on measurement of spectral-domain optical coherence tomography parameters. Br J Ophthalmol. 2015 Jan;99(1):69-74.

Sommer A, Katz J, Quigley HA, Miller NR, Robin AL, Richter RC, et al. Clinically detectable nerve fiber atrophy precedes the onset of glaucomatous field loss. Arch Ophthalmol. 1991; 109: 77-83.

Sung MS, Kang YS, Heo H, Park SW. Characteristics of optic disc rotation in myopic eyes. Ophthalmology. 2016 Feb;123(2):400-407.

Takasaki H Higashide T Takeda H Ohkubo S Sugiyama K. Relationship between optic disc ovality and horizontal disc tilt in normal young subjects. Jpn J Ophthalmol . 2013; 57: 34-40.

Tay E, Seah SK, Chan SP, Lim AT, Chew SJ, Foster PJ, Aung T. Optic disk ovality as an index of tilt and its relationship to myopia and perimetry. Am J Ophthalmol. 2005 Feb;139(2):247-52.

Valverde-Megías A, Martinez-de-la-Casa JM, Serrador-García M, Larrosa JM, García-Feijoó J. Clinical relevance of foveal location on retinal nerve fiber layer thickness using the new FoDi software in spectralis optical coherence tomography.Invest Ophthalmol Vis Sci. 2013 Aug 27;54(8):5771-5776.

Wang G, Qiu KL, Lu XH, Sun LX, Liao XJ, Chen HL, Zhang MZ. The effect of myopia on retinal nerve fibre layer measurement: a comparative study of spectral-domain optical coherence tomography and scanning laser polarimetry. Br J Ophthalmol. 2011 Feb;95(2):255-260.

Williams KM, Verhoeven VJ, Cumberland P, Bertelsen G, Wolfram C, Buitendijk G.H, ... & Höhn, R. (2015). Prevalence of refractive error in Europe: the European eye epidemiology (E3) Consortium. European journal of epidemiology, 30(4), 305-315.

Yamashita T, Asaoka R, Kii Y, Terasaki H, Murata H, Sakamoto T. Structural parameters associated with location of peaks of peripapillary retinal nerve fiber layer thickness in young healthy eyes. PLoS One. 2017 May 25;12(5):e0177247. doi: 10.1371/journal.pone.0177247.

Yamashita T, Asaoka R, Tanaka M, Kii Y, Yamashita T, Nakao K, Sakamoto T. Relationship between position of peak retinal nerve fiber layer thickness and retinal arteries on sectoral retinal nerve fiber layer thickness. Invest Ophthalmol Vis Sci. 2013 Aug 13;54(8):5481-5488.

Yamashita T, Sakamoto T, Terasaki H, Tanaka M, Kii Y, Nakao K. Quantification of retinal nerve fiber and retinal artery trajectories using second-order polynomial equation and its association with axial length. Invest Ophthalmol Vis Sci. 2014 Jul 29;55(8):5176-5182.